Indian Journal of Engineering & Materials Sciences
Vol. 30, June 2023, pp. 365-368
DOI: 10.56042/ijems.v30i3.3666

Tailoring the Properties of Nanocrystalline Tin(II) Selenide Films through Precursor Concentration Modulation

Deep Shikha[a], Vimal Mehta[a*], Mahesh Kumar[b], & R P Chauhan[c]

[a]Department of Physics, Sri Guru Teg Bahadur Khalsa College, Anandpur Sahib 140 118, India

[b]Principal Scientist, National Physical Laboratory, New Delhi 110 012, India

[c]Department of Physics, National Institute of Technology, Kurukshetra 136 119, India

Received: 10 May 2023; Accepted: 30 May 2023

An X-ray diffractometer for structural, a UV-VIS Spectrophotometer for optical, and a unique aluminium sample holder intended to examine the electrical properties of the synthesized SnSe thin films on non-conductive glass substrates in an alkaline medium were used. Light shining through a transparent glass window illuminated the samples to examine their electrical (photoconductivity) properties. The XRD results show that all of the films are orthorhombic crystals. The concentration of the precursor affects microstructural characteristics such as micro strain, crystallite size, and dislocation density. SnSe thin films' optical bandgap is measured using absorbance measurements. Semiconducting properties are confirmed by measuring the electrical conductivity, which reaches its highest value at the optimal precursor concentration. The as-grown SnSe films exhibit tunable photo response properties, which boost the practical application of the films in photovoltaic and solar cells.

Keywords: Chemical bath deposition, Thin Films, Tin selenide, Precursor, X-Ray Diffractometer (XRD)

1 Introduction

Consumption of energy has increased gradually with civilization. Energy crises have led to an increased focus on renewable energy sources since fossil fuel supplies are drying out and carbon dioxide emissions are growing. More electrical energy consumption is projected in the future to support human progress[1]. Solar cells hold great hope as a renewable energy source that is both environmentally friendly and economically viable.

The quest for thin-film materials for harnessing renewable energy through the conversion of solar energy and other related applications has lately escalated, using SnSe being one of the absorber substances. Silicon-based solar cell technology dominates the solar cell industry. Compared to direct band gap materials, silicon cannot absorb much sunlight due to its indirect band[2]. Metal chalcogenides, especially SnSe thin films, have gotten much attention because of their excellent performance compared to other materials[3]. Various researchers have created metal chalcogenides in the form of thin films.

A thin film deposition technology that can be conveniently handled cheaply is required for the large-scale manufacture of solar cells[4-5]. SnSe thin films were grown using a variety of evaporation mechanisms, including vacuum[6], flash[7], and reactive[8]. Several alternative processes are being employed for this purpose, including hot wall epitaxy[9], laser ablation[10], chemical bath deposition[11], and brush plating[12]. In contrast, most of these technologies are expensive and involve harmful substances, resulting in various technical and environmental difficulties. Chemical bath deposition is a straight forward, affordable, and practical method for creating high-quality films for device applications. In this study, SnSe films were made using the chemical bath deposition method with different concentrations of stannous chloride as a precursor, and their different properties were studied.

2 Materials and Methods

Glass with spectroscopic properties and research-grade chemicals was used to create thin layers of tin(II) selenide using chemical bath deposition (CBD). Tin(II) chloride and sodium selenosulfate were essential in providing Sn^{2+} and Se^{2-} ion precursors. It took about 10 hours of refluxing at 80°C with 5 g of selenium in 200 ml water to make 15 g of sodium sulfite solution. Throughout the reflux phase, the

*Corresponding author (E-mail: vimal78mehta@gmail.com)

mixture continued to be stirred continuously. The following is the reaction that must take place in order to make selenosulphate:

$$Na_2SO_3 + Se \rightarrow Na_2SeSO_3 \quad \ldots (1)$$

The unreacted selenium is removed using a filter, and the selenosulphate solution is stored in a hermetically sealed container. It is suggested that only modest quantities of the selenosulphate stock solution be prepared so that it may be utilized within three to four days.

The formation of a SnSe thin film begins with the dissolution of one mole of sodium hydroxide in deionized water. That mixture was used to keep an alkaline medium with a pH of around 11.4 at a constant level. In a beaker with a capacity of 100 millilitres, 9.4 mg of tin chloride was mixed with 10 millilitres of water, and then 11.4 millilitres of sodium hydroxide were added drop by drop.

Vertically lay glass substrate in bath, and then add 10 ml of sodium selenosulphate solution. The 45^{O}C temperature was used to grow the film. An initially dark brown precipitate becomes black after around 20 minutes. The beaker was left alone for nearly 2 h for the deposition process to grow the film. Filtration and drying in a hot oven separate SnSe from the remaining solution and produce a powdered form. This solid phase (powder) consists of SnSe nanocrystals.

At λ = 1.54060 Å, intensity versus 2θ diffraction patterns were recorded with an XPERT-PRO diffraction machine (40 mA, 45 kV) having CuKα_1 X-ray beam. Absorption spectra from 300-800 nm were recorded using double beam spectroscopy. Films are electrically measured in a metallic sample holder, as illustrated in Fig. 1, with light shining through a clear glass window. Photoconductivity experiments use a 200W, 8450-lx tungsten light. A 10^{-3} mbar vacuum is sustained during these experiments.

3 Results and Discussion

The XRD patterns were collected with XPERT-PRO diffraction equipment, and diffraction lines of SnSe were observed at $2\theta = 23.58^0$, 31.77^0, 32.78^0, $34.32^0$and 45.62^0 for thin films. The reported d-values for SnSe thin films closely conform with the orthorhombic structural standard values. The Full Width Half Maximum (FWHM) (β) can be related to strain (ε) and crystallite size (D) as[13]:

$$\frac{\beta Cos\ \theta}{\lambda} = \frac{1}{D} + \varepsilon \frac{Sin\ \theta}{\lambda} \quad \ldots (2)$$

The plots of $\beta(\cos\theta)/\lambda$ vs $(\sin\theta)/\lambda$, at various concentrations of precursor are shown in Fig. 2. The reciprocal of the intercept on the y axis in this graph will provide the particle size, and the slope of this graph will give the strain value. The particle sizes were 5.099 nm, 4.552 and 2.418 nm at 0.84g, 0.94g, and 1.04g concentrations of $SnCl_2$ precursor, respectively, and are shown in Table 1.

Increased crystallinity is seen from the rise in particle size from 2.418 to 5.099 nm at lower concentrations. The values of strain are also given in

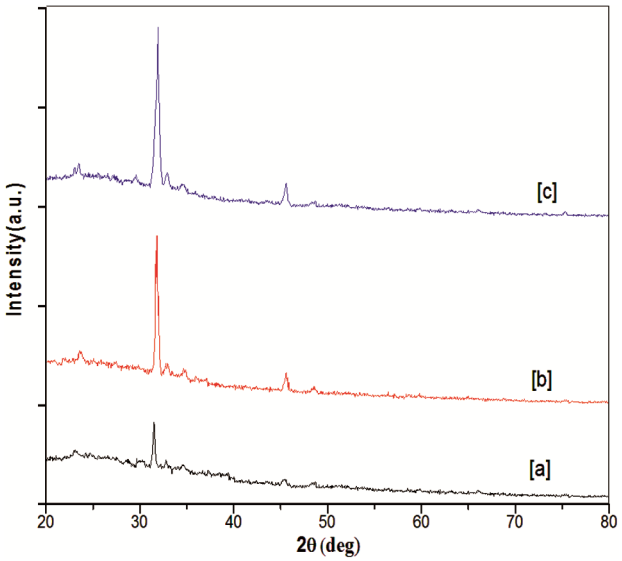

Fig. 1 — XRD spectra of SnSe thin films formed at various precursor concentrations: (a) 0.84g, (b) 0.94g, and (c) 1.04g.

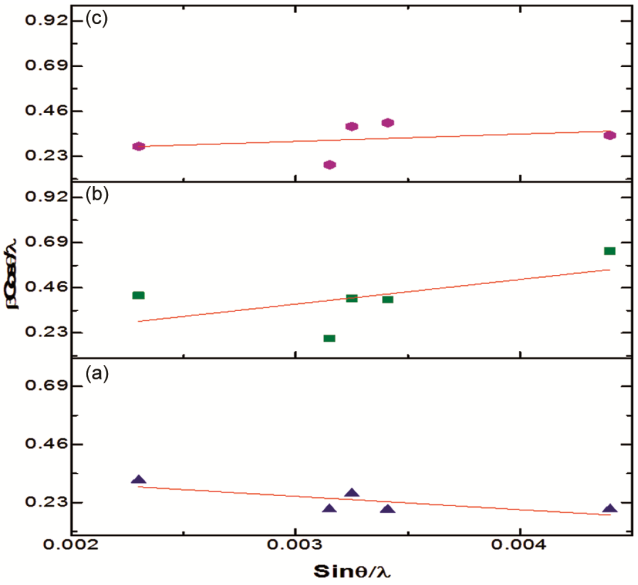

Fig. 2 — Size and strain graphs of SnSe thin films formed at various precursor concentrations: (a) 0.84g (b) 0.94g, and (c) 1.04g.

Table 1 — Structural characteristics of SnSe thin films formed at various precursor concentrations

Concentration (g)	Particle Size (nm)	Stress	Dislocation Density (m^{-2})	Band Gap (eV)
0.84	5.099	37.043	3.84 X10^{16}	2.14
0.94	4.552	125.553	4.82 X10^{16}	2.19
1.04	2.418	-53.02	1.71 X10^{16}	2.35

Table 1. Because the films produced at differing concentrations have negative residual strain values, this indicates the compressive strain. Compressive strain is generated at the thin film substrate interface when small crystallites adhere to the substrate due to surface tension in an impurity-free film.

δ, the dislocation density, may be found using[13] [3]:

$$\delta = \frac{1}{D^2} \quad \ldots (3)$$

The absorbance spectrum of thin films with varying concentrations is shown in the Fig. 3. The primary absorbance in a material that results in a transition from the valance band to the conduction band helps get the band gap. The absorption coefficient (α) and incoming photon energy (hv) are related as[14]:

$$\alpha = \frac{A\left(h\nu - E_g\right)^n}{h\nu} \quad \ldots (4)$$

where A is a constant, E_g is the material's energy band gap, and n is a transition-type exponent. The n may take on values of 1/2, 2, 3/2, and 3 for transitions such as "allowed direct," "allowed indirect," "forbidden direct," and "forbidden indirect.".

Equation 4 is used to get the direct optical band gap energy, denoted by the symbol "E_g". The $(\alpha h\nu)^2$ against hv graph curves (Fig. 4) were extrapolated to get the band gap.

Table 1 contains the proper values of E_g, calculated at various concentrations. E_g reduces as precursor concentration rise. It is because particle size increases as concentration increases. Because of the quantum confinement that occurs in SnSe nano-crystallites, the measured values of E_g have a greater significance than the bulk optical gap, which is 1.3 eV[15].

Upon placing the grown films in the specifically designed holder, the dark conductivity (σ_d) assessments were carried out. Analyzing the DC conductivity of semiconductors may reveal a great deal about their underlying conduction process. According to the Arrhenius relation, the dark conductivity of SnSe is activated at higher temperatures[16,17]

$$\sigma_d = \sigma_0 \exp\left(-\Delta E_d / K_B T\right) \quad \ldots (5)$$

where ΔE_d is "dc conductivity activation energy", σ_0 is the "pre-exponential factor", and K_B is

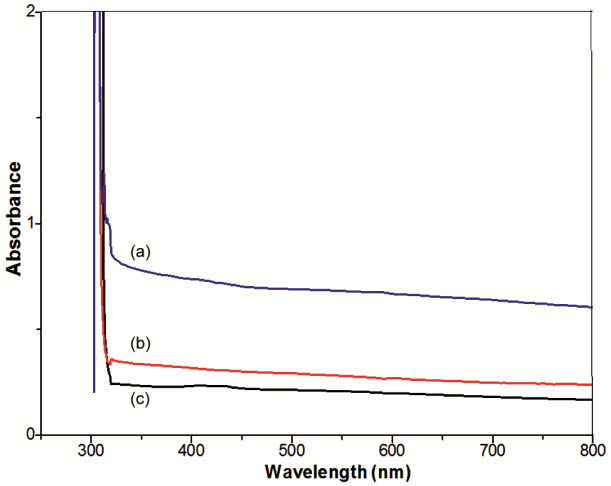

Fig. 3 — Absorbance versus wavelength graphs of SnSe thin films formed at various precursor concentrations: (a) 0.84g, (b) 0.94g, and (c) 1.04g.

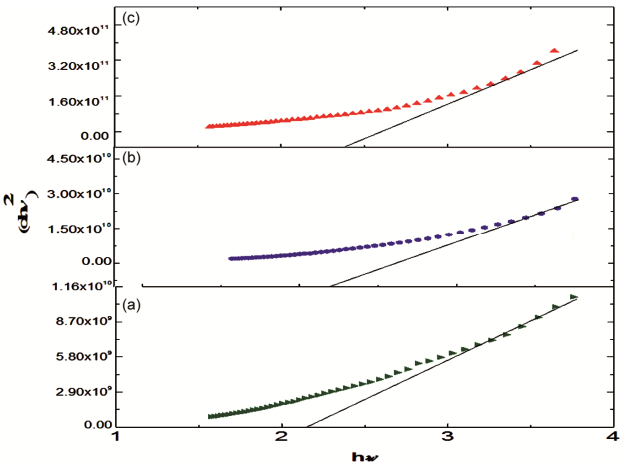

Fig. 4 — $(\alpha h\nu)^2$ vs energy graphs for SnSe thin films formed at various precursor concentrations: (a) 0.84g, (b) 0.94g, and (c) 1.04g.

"Boltzmann's constant". Table 2 provides Fig. 5 slope-based dark conductivity and activation energies. At varying precursor concentrations, nanocrystalline SnSe thin films exhibit temperature-dependent photoconductivity (Fig. 6). Equation 5, provides the photoconductivity (σ_{ph}) and the photoactivation energies (ΔE_{ph}) values which are shown in Table 2. Photoconduction activation energies are significantly lower than the similar dark conduction values. Temperature measurements have not shown a steady-

Table 2 — Electrical parameters for SnSe thin films formed at these various precursor concentrations of [a] 0.84g [b] 0.94g and [c] 1.04g

Conc.	σ_d ($\Omega^{-1}cm^{-1}$)	E_d (eV)	σ_{ph} ($\Omega^{-1}cm^{-1}$)	E_{ph} (eV)	σ_{ph}/σ_d
0.84g	1.125 X 10^{-6}	0.75	1.00 X 10^{-5}	0.61	8.88
0.94g	6.154 X 10^{-6}	0.66	1.506 X 10^{-6}	0.57	2.44
1.04g	9.173 X 10^{-6}	0.62	2.87 X 10^{-6}	0.54	3.12

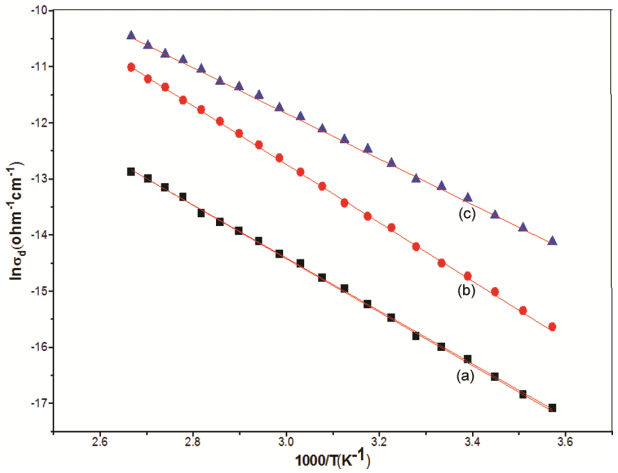

Fig. 5 — ln σ_d vs 1000/T graphs of SnSe formed at various precursor concentrations: (a) 0.84g, (b) 0.94g, and (c) 1.04g.

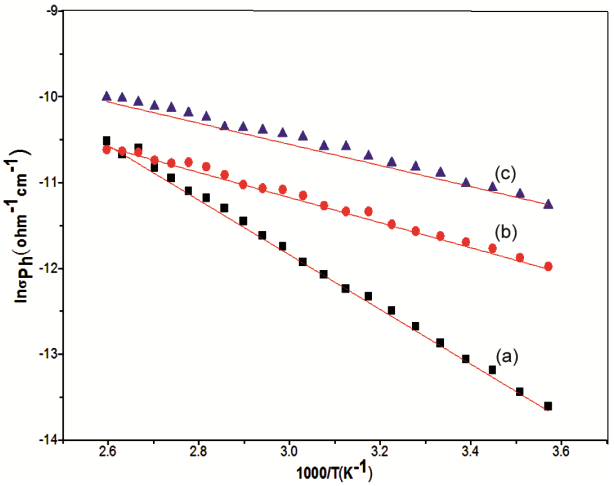

Fig. 6 — ln σ_{ph} vs 1000/T graphs of SnSe films formed at various precursor concentrations: (a) 0.84g, (b) 0.94g, and (c) 1.04g.

state photoconductivity maximum. The value of photosensitivity (Table 2) has also been found.

4 Conclusion

Chemical bath deposition at varying precursor concentrations produces nanocrystalline SnSe thin films. Comparing all samples' d-values to the standard supports SnSe's orthorhombic structure. Average crystallite size decreases with increasing $SnCl_2$ precursor concentration. All samples are strained owing to surface tension. SnSe thin films with varied precursor concentrations have a direct optical band gap. The confinement effect resulting from a decrease in crystal size in the grown nanocrystalline samples is responsible for a blue shift in the fundamental edge. All samples' dark conductivity, photoconductivity, activation energies, and photosensitivity were computed. Its high absorption coefficients and low electrical resistance make SnSe an excellent thin-film solar cell absorber, and its properties (precursor concentration) may be modified to make it work in solar cells.

Acknowledgement

The authors would like to acknowledge the financial support received for this work under DST-FIST Scheme (No. SR/FST/College-2019-759(C)) and DBT-Star College Status Scheme (No. HRD-11012/4/2022-HRD-DBT). We would also like to thank all the staff members of the Department of Physics for their valuable assistance during the course of this study.

References

1 Kuo-Jui, H, *Electron-Reflector strategy for CdTe thin-film solar cells PhD Thesis. Colorado State University, Department of Physics*, USA 2010.
2 Fahrenbruch, *A L and Bube R H, Fundamentals of solar cells New York Academic Press*, USA 1983.
3 Deep Shikha, Vimal Mehta, Jeewan Sharma and R P Chauhan, *J Mater Sci Mater Electron,* 28, (2017), 2487.
4 Mariappan, R, Ragavenda M and Gowrisankar G, *Chalcogenide Lett* , 7(2010), 211.
5 K. Zweibel, *Sol Energy Mate Sol Cells,* 63 (2000), 375.
6 D.T. Quan, *Thin Solid Films* 149 (1987) 197.
7 J.P. Singh, R K Bedi *Thin Solid Films*, 199 (1991), 9.
8 J P Singh, R K Bedi *J Appl Phys*, 68(1990), 2776.
9 R Teghil, A Santagata, V Marotta, S Orlando, G Pizzella, A Giardini Guidoni, A Mele, *Appl Surf Sci*, 90 (1995), 505.
10 B Subramanian, C Sanjeeviraja, M Jayachandran, *J Crystal Growth*, 234 (2) (2002), 421.
11 Deep Shikha, Jeewan Sharma, J Sharma, *J Optoelectron Adv Mater,* 18(1-2) (2016), 130.
12 Z Zainal, N Saravanan, K Anuar, M Z Hussein, W M M Yunus, *Materials Science* and *Engineering B,* 107, (2004), 181.
13 Deep Shikha, Vimal Mehta, Jeewan Sharma, R.P. Chauhan, *Journal of Material Science Mater Electron,* 28, (2017), 8359.
14 Vimal Mehta, Deep Shikha, Jeewan Sharma, R P Chauhan, *Journal of Material Science Mater Electron*, 29, (2018), 8801.
15 Weiran Shi, Minxuan Gao, Jinping Wei, Jianfeng Gao, Chenwei Fan, Eric Ashalley, Handong Li and Zhiming Wang, *Adv Sci,* 5(4), (2018), 1700602.
16 Jeewan Sharma, Deep Shikha, S.K. Tripathi, *Romanian Reports in Physics,* 66(4), (2014) 1002.
17 Deep Shikha, Vimal Mehta, R.P. Chauhan, *Opt. Mater,* 126, (2022), 112093.